Pattern Recognition on X-ray Fluorescence Records from Copenhagen Lake Sediments Using Principal Component Analysis

Norman Schreiber · Emanuel Garcia · Aart Kroon · Peter C. Ilsøe · Kurt H. Kjær · Thorbjørn J. Andersen

Abstract Principal component analysis (PCA) was performed on chemical data of two sediment cores from an urban freshwater lake in Copenhagen, Denmark. X-ray fluorescence (XRF) core scanning provided the underlying datasets on 13 variables (Si, K, Ca, Ti, Cr, Mn, Fe, Ni, Cu, Zn, Rb, Cd, and Pb). Principal component analysis helped to trace geochemical patterns and temporal trends in lake sedimentation. The PCA models explained more than 80 % of the original variation in the datasets using only two or three principal components. The first principal component (PC1) was mostly associated with geogenic elements (Si, K, Fe, Rb) and characterized the content of minerogenic material in the sediment. In the case of both cores, PC2 was a good descriptor emphasized as the contamination component. It showed strong linkages with heavy metals (Cu, Zn, Pb), disclosing changing heavy-metal contamination trends across different depths. The sediments featured a temporal association with contaminant dominance. Lead contamination was superseded by zinc within the compound pattern which was linked to changing contamination sources over time. Principal component analysis was useful to visualize and interpret geochemical XRF data while being a straightforward method to extract contamination patterns in the data associated with temporal elemental trends in lake sediments.

Keywords Urban lake sediment · Contamination · Heavy metals · XRF · PCA

N. Schreiber (✉) · A. Kroon · T. J. Andersen
Department of Geosciences and Natural Resource Management, University of Copenhagen,
Øster Voldgade 10, 1350 Copenhagen K, Denmark
e-mail: nos@ign.ku.dk

E. Garcia
Department of Food Science, Section of Spectroscopy and Chemometrics, University of Copenhagen,
Rolighedsvej 30, 1958 Frederiksberg, Denmark

E. Garcia
Center for Herd-oriented Education, Research and Development (HERD), Department of Large Animal Sciences, University of Copenhagen,
Grønnegaardsvej 2, 1870 Frederiksberg, Denmark

P. C. Ilsøe · K. H. Kjær
Center of GeoGenetics, Natural History Museum of Denmark, University of Copenhagen,
Øster Voldgade 5-7, 1350 Copenhagen K, Denmark

1 Introduction

Urban environments feature strong imprints of human activity. They are centers of industrial growth and economical production, wherefrom contaminants like heavy metals are intensively emitted since the beginning of the Industrial Age (Crutzen 2002; Lyons and Harmon 2012). In recent times, this contamination is constantly surveyed by air quality monitoring programs (Ellermann et al. 2012), and it is decreasing in many industrialized countries (von Storch et al. 2003). In contrast, past environmental burdens can only be indirectly assessed. Particularly, lake sediment strata have proven to be a useful tool for contamination investigations as they serve as final sinks for these contaminants

in aquatic environments and thus function as historical archives (Haworth and Lund 1984; Last and Smol 2004). Both urban and remote lacustrine locations contain distinct anthropogenic impacts (Renberg 1986; Chillrud et al. 1999; Walraven et al. 2014).

X-ray fluorescence (XRF) core scanning has become widely used to assess sedimentary element levels, especially since the early 2000s (Croudace et al. 2006). It provides an effective technique to generate large datasets covering major and trace elements (Weltje and Tjallingii 2008; Comero et al. 2011; Löwenmark et al. 2011). On the one hand, iron (Fe), titanium (Ti), and silicon (Si) as well as alkali metals such as rubidium (Rb) and potassium (K) are prominent in clay minerals. They serve as ideal scavenger for heavy metals due to their large relative surface areas (Eisma and Irion 1988). On the other hand, elements like copper (Cu), zinc (Zn), lead (Pb), chromium (Cr), nickel (Ni), and cadmium (Cd) characterize anthropogenic imprints. They are mainly emitted by high temperature processes such as fossil fuel combustion and as part of material preservation applications (Nriagu 1979). Manganese (Mn) has redox-sensitive properties that can mark interactions at the water-sediment interface (Hallberg 1991; Davison 1993). Calcium (Ca) can be considered a salinity indicator, as it is the fifth most abundant element in seawater and could reveal occurrence of carbonate precipitation in the sediment columns.

For associated data interpretation, applications of multivariate statistics have proven to be a beneficial tool to apply on records in order to e.g. group variables of similar characteristics and properties (Selig and Leipe 2008; Templ et al. 2008; Hansson et al. 2013). Principal component analysis (PCA) is a powerful method used in chemometrics which provides an overview of complex multivariate data, revealing relations between variables and samples (Bro and Smilde 2014). Its application on environmental data is well documented revealing basic relationships in element data and providing data association and dimension reduction (Zitko 1994; Zupan et al. 2000; Passos et al. 2010; Gredilla et al. 2012). Furthermore, it serves for pattern recognition, for outlier detection, and for data classification and trend delineation (Wold et al. 1987; Olsen et al. 2010; Comero et al. 2011; Quinn and Keough 2013).

In this study, PCA implementation on 13 variables of XRF core scanning from a lake in the center of Copenhagen is presented in order to detect features and nature of heavy metal contamination in an urban environment. A number of cores were retrieved from lakes in the former defense work system and cores from one site, the Botanical Garden, proved to be particularly well preserved (Fig. 1). The lake and its sediments from the heart of Copenhagen were therefore chosen as investigation site as it could provide detailed information since its establishment in the seventeenth century. The

Fig. 1 Maps showing (a) North-Western Europe, (b) Copenhagen City center, and (c) the coring sites in the lake of the Botanical Garden of Copenhagen
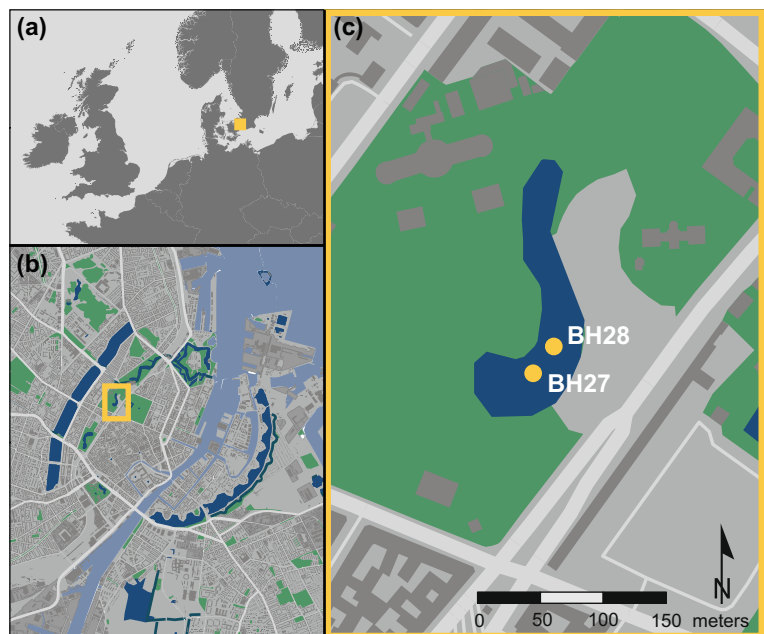
Danish capital has been a center for trading in Baltic region since the Middle Ages and was therefore exposed to a large variety of power and goods at an early stage. Since a historical contamination reconstruction is intended, underlying chemical patterns are highlighted and linked to their sources.

2 Material and Methods

Two sediment strata were retrieved from the central part of lake within the Botanical Garden of Copenhagen, Denmark (55° 41 10 N, 12° 34 28 E). The cores BH27 (145 cm long) and BH28 (138 cm long) were taken circa 30 m from each other using a rod-operated piston corer (Livingstone 1955; Smol 2008). The corer consisted of a tube sealed with a piston which was attached to an extension rod. This construction was lowered through the water column onto the sediment surface. Subsequently, the tube was penetrated through the sediment column until a coarse, sandy bottom was reached. The coring was done in winter 2011, and sediment recovery was achieved through holes in the ice-covered lake. The examined water body once belonged to a late medieval moat as part of the defense-wall system established around AD 1650 and surrounding the old town (Skaarup et al. 1998). It was turned into a lake by partial terrain leveling along with urban expansion since the mid-nineteenth century. There is no historical or sedimentological data indicating that the lake has been dredged, but the establishment of the Botanical Garden between 1872 and 1874 (Skaarup et al. 1998) appears to have induced an elevated input of minerogenic material leaving behind a chronological time-marker (see later). Today, the freshwater lake has a surface area of approximately 7000 m^2 and a maximum water depth of about 2 m. Lake-water temperature varies with air temperature, so that the water body's surface even freezes in winter time.

The cores were permanently stored at 4 °C. The sediment tubes were split in halves and analyzed at the Department of Geological Sciences at Stockholm University, Stockholm, Sweden, using an Itrax™ X-ray fluorescence (XRF) core scanner (COX Analytical Systems 2011). This nondestructive technique provided datasets of major elements and trace elements as well as line-scan images and radiographs (XRG; line-scanned) of the sediment cores (Croudace et al. 2006). Therefore, the core halves were covered with a thin polyethylene

film. The XRF-core scanner was used in combination with a 3 kW molybdenum (Mo) tube operating at 55 kV and 50 mA. Especially, elements of environmental interest were detected in this way due to their relatively low detection limits (Croudace et al. 2006). The measurements were acquired at a 1000-μm increment with an exposure time of 200 ms.

The obtained datasets were auto-scaled by subtracting the overall average ($\bar{x}$) from each variable and dividing by the standard deviation (σ) which resulted in datasets with a new mean of zero ($\bar{x}_a$) and a standard deviation of 1 (σ_a) (Eq. 1). This form of data rescaling provided intercomparable objects of all variables for all associated cores on the one hand and removed the influence of extreme values on the PCA results on the other hand (Zitko 1994; Quinn and Keough 2013; Bro and Smilde 2014).

$$\frac{x - \bar{x}}{\sigma} \Rightarrow \bar{x}_a = 0; \ \sigma_a = 1 \qquad (1)$$

Light intensity was calculated as well in order to facilitate the detection of matrix differences in the sediment columns. From the monochromatic radiograph images, a maximum of 256 shades of gray were read by automatically allocating one value between 0 (for black) and 255 (for white) to every pixel.

Variable selection for the principal component analysis was based on environmental interest and geochemical properties. Here, multivariate statistical methods have some significant advantages over univariate techniques as they account for a group of variables that influence the data variability jointly (Borůvka et al. 2005). Even though environmental, geochemical data usually contains strong correlations, PCA contributes with its exploratory approach and decreases the data dimensionality while retaining most of the original information. On the basis of chosen variables, e.g., chemical elements, PCA provided their weights gathered in compound variables, the principal components (PC) which best explained the data variation (Bro and Smilde 2014). These components are independent in their contribution to the explained variation as they are orthogonal (Bro and Smilde 2014). The first PC explained the largest variation in the datasets in a certain multidimensional direction and every subsequent component accounted for additional information. A scree plot showed how much of the original variance in the dataset was explained by each PC. From this point on,

Fig. 2 Radiograph image (XRG) and auto-scaled data for light intensity by depth for cores (**a**) BH27 and (**b**) BH28. Value *0* marks the scaled data average
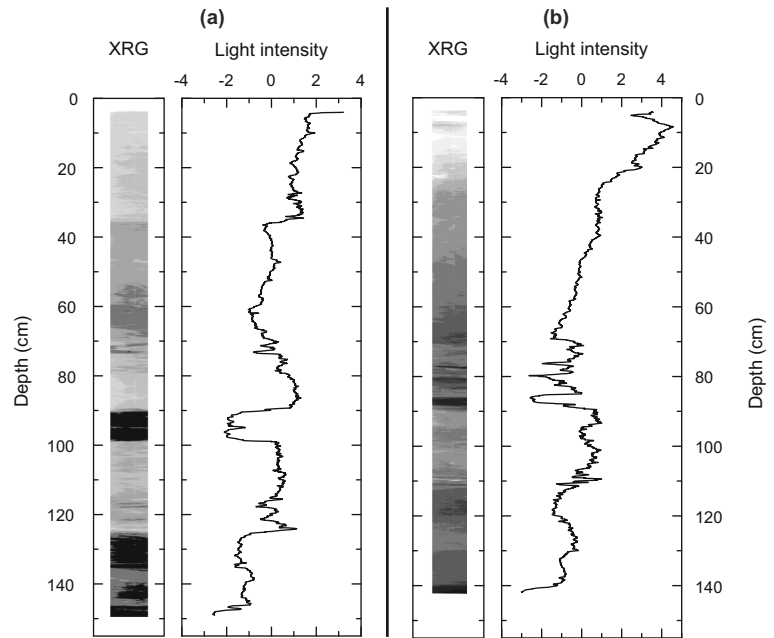
the number of principal components was chosen which shall retain in the PCA model. On this basis, a score plot was developed which structured the representation of the original samples in the new multidimensional space, whereas the loadings plot highlighted the contribution of the variables to the principal components. In general, high loadings of elements express their importance for the PC. Score and loadings plots always have to be interpreted together. Avoiding consideration of textural differences in the PCA models fundamentally increased the description of it (Reid and Spencer 2009).

3 Results

The deposits of the lake within the Botanical Garden of Copenhagen are muddy. In both cores, two distinct layers are interstratified in the sediment columns, referred to as M1 and M2, indicating changes in the accumulation regime (Fig. 2; XRG panels). Both substrates were visually recognized by a change in material color from grayish-/brownish-green to yellowish-/greenish-gray. For BH27, M1 occurred between 61 and 71 cm, whereas M2 appeared between 89 and 99 cm. In core BH28, these layers did not appear quite as thick with M1 between 62 and 71 cm and M2 at around 86.5 cm.

Textural changes were also identified on the basis of light intensity as it is a direct function of material density. Light intensity was determined by the individual radiograph images. Figure 2 shows these radiographs and the related auto-scaled light intensity for core BH27 and BH28. Auto-scaled light intensity values steadily increased from the bottom to the top of core BH27 (Fig. 2a). This course is interrupted by a distinct decrease between 99- and 92-cm depth. At around 38-cm depth, values shift from measurement mean to 1.6 σ and continued at this level until core surface. In the case of BH28 (Fig. 2b), auto-scaled light intensity revealed a distinct maximum at 86.5 cm. Strongly varying material density differences were recognized up to a depth of 68 cm. From there on, values steadily increased to the sediment surface.

Figure 3 depicts the auto-scaled element data for core BH27 over depth. Silicon, K, Ti, Fe, and Rb values showed a major deviation from their overall progression at the core bottom as well as at the depths between 89 and 99 cm. This tendency was also obvious in the Cd trend to a moderate degree.
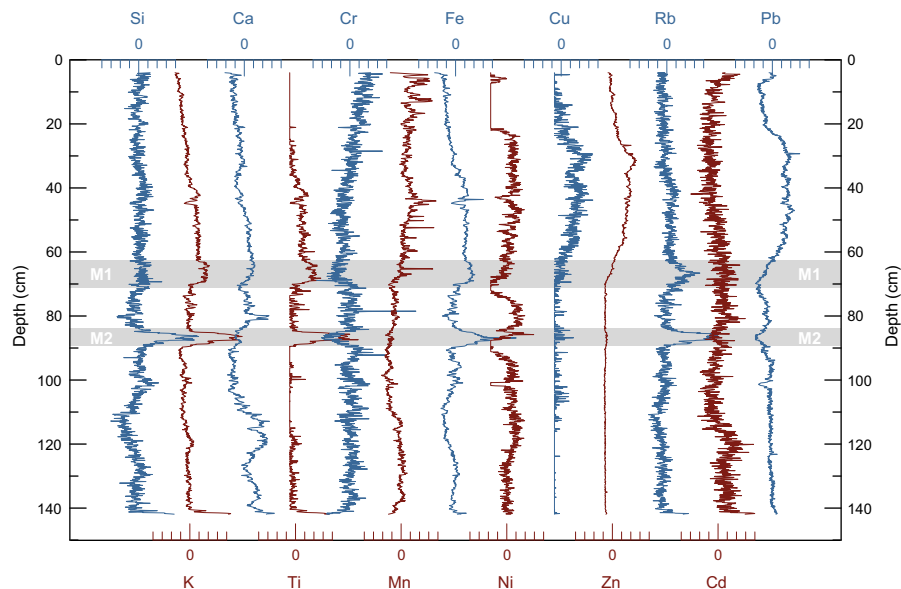
Auto-scaled element data for core BH28 over depth is depicted in Fig. 4. Also for this core, Si, K, Ti, Fe, and Rb values showed a major shift from their overall course at the core bottom as well as at the depths between 83 and 89 cm. This tendency was associated with a decrease in Cr values at these depths.
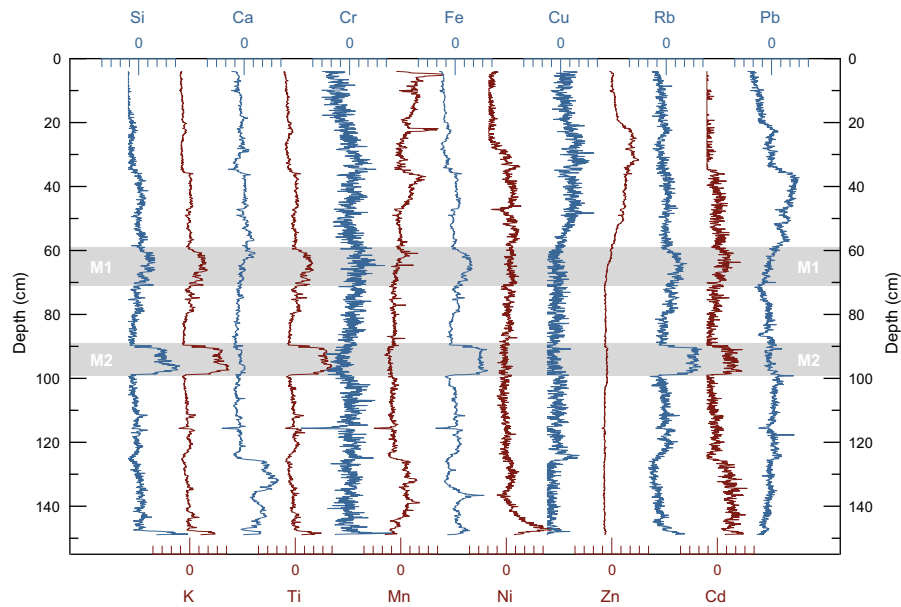
Fig. 3 Auto-scaled data of XRF measurements over depth for core BH27. Value *0* marks the scaled data average, whereas every *tick mark* represents one standard deviation

The primary objective of the study was to examine whether PCA could help to visualize changing contamination patterns over core depth. Therefore, an initial PCA on the entire core (*full core model*) was run to identify the textural changes on elemental basis that also became visible in the light intensity data. Furthermore, general contaminant features should be accentuated.

Subsequently, a second PCA (*top core model*) was carried out covering only the top part of the cores in order to avoid the influence with markedly textural differences on the PCA result. The distinction of these core sections was based on the element and light intensity profiles, the lower parts of the core sections were then excluded, and the data columns were auto-scaled

Fig. 4 Auto-scaled data of XRF measurements over depth for core BH28. Value *0* marks the scaled data average, whereas every *tick mark* represents one standard deviation

without these data (Wold et al. 1987; Quinn and Keough 2013). This way, more homogenous core segments were considered. The *top core PCA model* was calculated afterward which covered the same variables only for the upper, homogenous part of the cores.

Principal component 1 of the *top core model* of BH27 already accounted for 60 % of the datasets variations, whereas PC1 of the *full core model* captured 46 %. The explained variance for PC2 increased from the *full core model* to the *top core model* as well, from 18 to 20 %, respectively. At least three principal components would be required in order to reach about 80 % explanation for the *full core model*, whereas only two were required in the *top core model*.

The first PC of the *full core model* of BH28 captured only 40 %, whereas PC1 of the *top core model* accounted for 47 %. Principle component 2 captured 26 % in the *full core model* and 29 % after data restriction. Again, the explanatory strength was increased from the *full core model* to the *top core model*. If the *full core model* should reach an equivalent acquisition as the *top core model*, at least three principal components would be required as well.

The loadings for the chosen chemical variables with the principal components are presented in Fig. 5. For both cores, BH27 (Fig. 5a) and BH28 (Fig. 5b), the first PC was strongly related to elements referring to clay minerals like Si, K, Ti, Fe, and Rb. In general, relations were strengthened from the *full core* to the *top core models*. In the case of BH27, minerogenic elements reached mean loadings of 0.91 in the *full core model* and 0.96 in the *top core model*. Cadmium also showed strong relations to this PC, although rather considered a contamination indicator instead. For BH28, clay mineral-related elements had a mean loading of 0.88 for the *full core model* and only 0.82 for the *top core model*. The *full core model* of BH27 described the contaminants with the use of the first three PCs. This was decreased to two principal components in the *top core model*. Strongest loadings were acquired for Cu, Zn, and Pb with an average of 0.82.
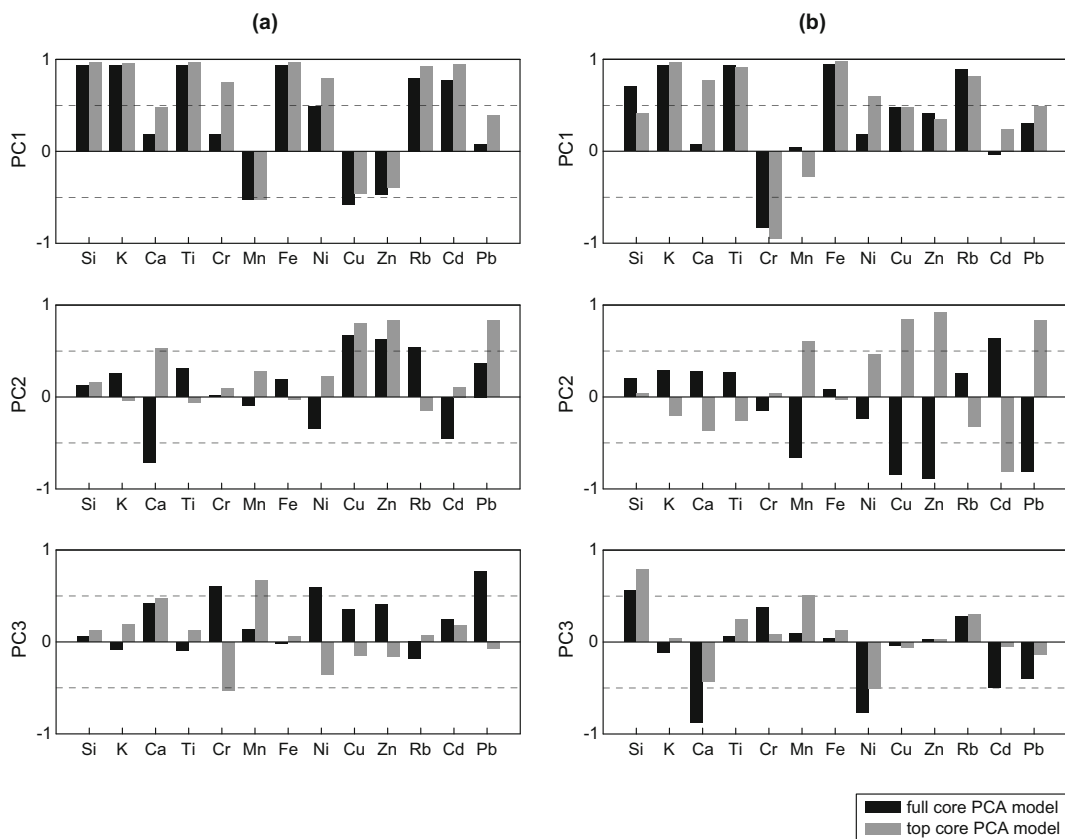
Fig. 5 Loadings of variables (weights) with the first three principal components for *full core* and *top core PCA models* of (**a**) core BH27 and (**b**) core BH28

The PCA models for BH28 always enclosed contaminants in the second principal component, although shifting from positive to negative loadings and vice versa. The image appeared mirrored and accounted to a switch of algebraic signs from the *full core* to the *top core PCA model* of this dataset due to associated outlier removal (Bro et al. 2008). Disregarding this arbitrariness in sign conventions (Bro et al. 2008), the amplitude of the loadings increased for Cu, Zn, and Pb. In addition, it covered a relatively high negative loading for Cd with −0.81.

Figure 6 compiles the loadings for PC1 and PC2 of core (a) BH27 and (b) BH28 over depth. Layer of textural difference was recognized by high positive standard deviations for the *full core model* of core BH27. They extended over 10 cm from 89 to 99 cm reaching values above 3 σ (PC1). This part was also recognized in the auto-scaled element data of the full core as well (Fig. 3). Below this part, several other depths (e.g., 123–135 cm) could be addressed the same way. In general, a decreasing trend for PC1 was obvious from the core bottom to the sediment surface which was interrupted by the responded M2 section and a layer with elevated values around 63-cm core depth (M1). The textural variation also became obvious in PC2. Its course started at around −2 σ and drastically increased to the mean at 130 cm. Interrupted by M2, this level was kept until around 60 cm. Here from, PC2 values increased to a maximum of 1.4 σ at 31.5 cm. The measurements returned to the mean level all the way up to the sediment surface. The continuing analysis

comprised depths from 0 to 85 cm only in order to avoid the influence of the described elevated values on the *top core PCA model*.

In the case of BH28, the first principal component features a distinct maximum at 86.5 cm with 4.6 σ which could be traced at PC2 as well. Principal component 2 of the *full core model* had negative loadings of the associated elements (see Fig. 5b) and therefore associated negative scores. In general, the depicted inverse scores were linked to concentration maxima. Values arranged along 1 σ until they start to increase at around 68 cm to their minimum at 30.5 cm with −2.2 σ. These measurements reached their mean again until the sediment surface. The depths from 0 to 80 cm were included for the *top core model* of BH28.

4 Discussion

The datasets being analyzed in detail comprised two cores of sediments from the lake of the Botanical Garden of Copenhagen. The rod-operated piston corer was penetrated as deep as possible into the sediment until a coarse, sandy bottom was reached. This signified that the complete strata covering lacustrine accumulations were retrieved.

Even though the two sediment cores featured macroscopic differences as seen on the XRG images (Fig. 2), their PCA models revealed similar patterns when highlighting clay minerals by the first principal component and heavy metal contamination by the second one

Fig. 6 Principal component scores by depth for the *full core model* of (a) BH27 and (b) BH28
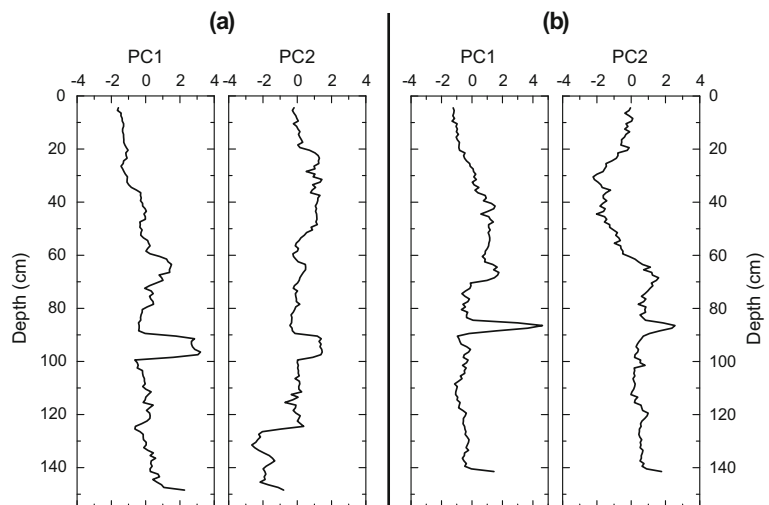
(Fig. 5). However, variable behavior depicted in calculated loadings appeared to be different when considering each individual core. The individual explanation of the PCs varied for the models although the variables showed the same tendencies. This was due to different sedimentological features as depicted in light intensity (Fig. 2; XRG panels). The full core models highlighted textural variation and covered all depths and their associated measurements. The *top core model* had the advantage to be restricted on the basis of dimensions and maintained a high level of explained variance as they contained a homogenous core section only. It was important to carry out an initial PCA on the full datasets as it revealed differences that immoderately shifted the model's depiction and facilitated in reducing the dimensionality even more. Along with this, density features of the investigated material as represented by light intensity help to restrict the model and improve its explanatory strength.

The thickness of the minerogenic layers (M1 and M2) could easily lead to an overestimation or underestimation of variables due to their associated chemical properties. Here, especially M2 stood out due to high values for PC1. Therefore, it was necessary to reduce the number of considered objects for further analysis. Other studies showed that a normalization of the data to a lithogenic element (Löwenmark et al. 2011) or to grain size (Reid and Spencer 2009) improved model recovery. Results for ideal normalization elements like aluminum (Al) were neglected due to the utilization of Mo tube in

the XRF analysis. Light elements in particular could be biased by absorption effect of water along with the use of a polyethylene film covering the core during the measurement (Kido et al. 2006; Tjallingii et al. 2007). In addition, surface roughness and density could affect XRF analysis (Croudace et al. 2006). In order to minimize these effects, the PCA result was instead controlled by choosing only the homogenous top sections of the sediments in the *top core PCA models* on the basis of element and light intensity data. For comparison, Reid and Spencer (2009) gained similar loading recovery when normalizing their environmental data by the fine sediment fraction (<63 μm).

A distinct trend over depth was visible when looking at the score plot in combination with the loadings plot for the *top core model* of core BH27 (Fig. 7). Samples starting from the M2 layer, around 85 cm, showed a tendency toward the natural component. This process climaxed in the depths around 60 to 70 cm and is related to the M1 layer samples. Lead dominated the pattern in depths above this level. At around 35 cm, this trend appeared to be superimposed by other contaminants, namely Cu and Zn. The sediment surface (0–20 cm) was dominated by the influence of redox-sensitive Mn which marked the water-sediment boundary.

A similar picture to Fig. 7 was drawn from the *top core model* of BH28 (Fig. 8). Depths from 60 to 70 cm were directly associated with the first component (PC1), while subsequent samples started to be dominated by the second component (PC2). Heavy metals like Cu, Zn,
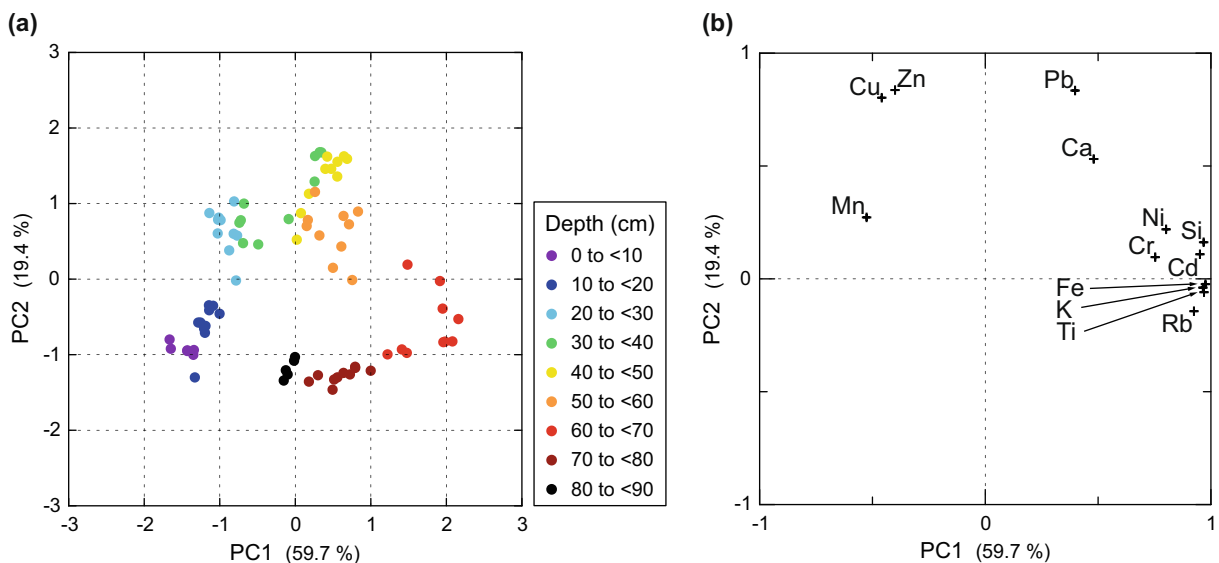
Fig. 7 The *top core PCA model* of core BH27 including (**a**) score and (**b**) loadings plot

and Pb had high levels especially between 30 and 50 cm. Sediment surface depths could only be associated with redox-sensitive Mn to a minor degree.

Explanatory power of the PCAs was increased by limiting the models to certain depths from the *full core model* to the *top core model*. In order to distinguish variables of highest importance for a principal component, we have set an overall loadings threshold of $r = 0.8$. This procedure facilitated the characterization of the compound variables. Thereby, the first PC could be addressed as the *natural component* since it had the strongest relationships with elements that refer to clay minerals and aluminosilicates. Silicon mainly originated from weathering processes along with its high loading for Ti (0.95, BH27) (Olsen et al. 2010). Rubidium and K showed strong loadings in both PCA models as they originate from the clay mineral fraction in particular (Vasskog et al. 2012). The second PC could be characterized as *contamination component* as it contained high loadings with heavy metals which are linked to anthropogenic influence.

A third principal component missed its importance in the *top core models* since two PCs already explained ~80 % of the variance in the dataset. The Kaiser criterion (eigenvalues > 1) is often discussed as a threshold for the number of principal components used in a model (Comero et al. 2011). But since two principal components covered a large share of the dataset variation, two principal component models were considered as they facilitated a two-dimensional visualization. Beyond, the

third PC did not feature strong loadings except for Mn or Si after the models were limited to the top core sections.

It was possible to capture trends in the contamination sources by the PCA models since element contribution varied over depths. Temporal shifts in Pb and Zn contaminations of flood plain sediments in South-Eastern Czech Republic were observed by Matys Grygar et al. (2012). In our PCA model, the influence of variables associated with contamination decreased in favor of another variable as depicted in the shift between Pb and Zn (Figs. 7 and 8). Copenhagen had gone through a transition from a city being influenced by Industrial Revolution in the eighteenth century until today where it is branded "green," due to its intended extended use of renewable energies (Danish Ministry of Climate, Energy and Building 2013; European Environment Agency 2014). Especially during the period from the 1920s to the early 1990s, Pb was extensively used as an additive to gasoline (tetra-ethyl lead) and was wide-rangingly emitted to the atmosphere (Nriagu and Pacyna 1988). Environmental legislation, such as the phasing out of Pb in gasoline and the improvement of fly ash filters in incineration plants (European Council 1975, 1987; von Storch et al. 2003), supplied the basis for decreasing stresses on human health as well (Molin Christensen and Holst 1988). As Zn levels remained on a relatively higher level, source contribution patterns must have changed. Fossil fuel combustion may no longer be its dominating origin as the use of galvanized metal products and fertilizers increased alongside.
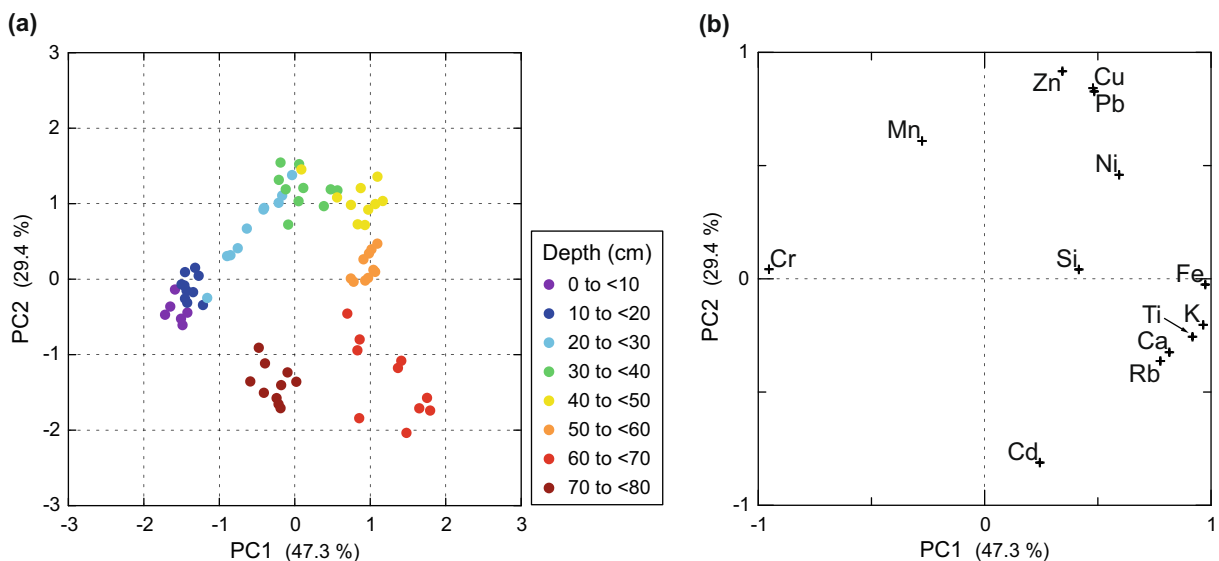
Fig. 8 The *top core PCA model* of core BH28 including (**a**) score and (**b**) loadings plot

Additionally, Zn-containing compounds are common constituents in hygienic products and agrochemicals and serve as wood preservation (Bhattacharya et al. 2002; Nicholson et al. 2003).

5 Conclusion

The application of principal component analysis (PCA) proved to be a helpful tool for interpreting XRF-core scanning datasets for the presented lacustrine cores. The number of variables of the presented datasets was considerably decreased from 13 measured elements to only two principal components while still capturing about 80 % of the original variance in the datasets. This aspect facilitated data presentation and its interpretation. Limiting the PCA models to only the homogenous top part of the cores, avoiding deeper layers with different texture, significantly improved the dimensionality of the PCA models.

The first and second principal components were related to sedimentological features and contamination burdens, respectively. Clay minerals dominated some parts of the core matrixes and were controlling the first principal component. Heavy metals in contrast were dominating the second principal component. Surprisingly, even the course of contamination trends were revealed by the help of the score plots, highlighting the transition of contamination loads over core depth and time in both locations.

Conflict of Interest No conflict of interest exists for any of the authors.

References

Bhattacharya, P., Mukherjee, A. B., Jacks, G., & Nordqvist, S. (2002). Metal contamination at a wood preservation site: characterisation and experimental studies on remediation. *Science of the Total Environment, 290*, 165–180.

Borůvka, L., Oldřich, V., & Jehlička, J. (2005). Principal component analysis as a tool to indicate the origin of potentially toxic elements in soils. *Geoderma, 128*, 289–300.

Bro, R., & Smilde, A. K. (2014). Principle component analysis. *Analytical Methods, 6*, 2812–2831.

Bro, R., Acar, E., & Kolda, T. G. (2008). Resolving the sign ambiguity in the singular value decomposition. *Journal of Chemometrics, 22*, 135–140.

Chillrud, S. N., Bopp, R. F., Simpson, H. J., Ross, J. M., Shuster, E. L., Chaky, D. A., Walsh, D. C., Choy, C. C., Tolley, L.-R., & Yarme, A. (1999). Twentieth century atmospheric metal fluxes into Central Park Lake, New York City. *Environmental Science and Technology, 33*, 657–662.

Comero, S., Locoro, G., Free, G., Vaccaro, S., De Capitani, L., & Gawlik, B. M. (2011). Characterisation of Alpine lake sediments using multivariate statistical techniques. *Chemometrics and Intelligent Laboratory Systems, 107*, 24–30.

Council, E. (1975). Council directive 75/442/EEC of 15 July 1975 on waste. *Official Journal of the European Communities, L194*, 39.

Council, E. (1987). Council directive 87/416/EEC of 21 July 1987 amending directive 85/210/EEC on the approximation of the laws of the member states concerning the lead content of petrol. *Official Journal of the European Communities, L225*, 33.

Cox Analytical Systems .(2011). ITRAX corescanner—unique multi-function scanner for core examinations. http://coxsys. se/wp-content/uploads/2009/03/itrax-core-scanner4.pdf. Accessed 04 June 2014.

Croudace, I. W., Rindby, A., & Rothwell, R. G. (2006). ITRAX: description and evaluation of a new multi-function X-ray scanner. *Geological Society, London, Special Publications, 267*, 51–63.

Crutzen, P. J. (2002). Geology of mankind. *Nature, 415*, 23.

Danish Ministry of Climate, Energy and Building. (2013). Smart grid strategy—the intelligent energy system of the future. http://www.kebmin.dk//klima-energi-bygningspolitik/dansk-klima-energi-bygningspolitik/energiforsyning-effektivitet/smart. Accessed 09 May 2014.

Davison, W. (1993). Iron and manganese in lakes. *Earth-Science Reviews, 34*, 119–163.

Eisma, D., & Irion, G. (1988). Suspended matter and sediment transport. In W. Salomons, B. L. Bayne, E. K. Duursma, & U. Förstner (Eds.), *Pollution of the North Sea—an assessment* (pp. 20–35). Berlin: Springer.

Ellermann, T., Nøjgaard, J.K., Nordstrøm, C., Brandt, J., Christensen, J., Ketzel, M., & Jensen, S.S. (2012). The Danish air quality monitoring programme. Annual Summary for 2011. Scientific Report from DCE – Danish Centre for Environment and Energy, 37.

European Environment Agency (EEA) .(2014). Copenhagen beats Bristol and Frankfurt to win European Green Capital 2014. http://www.eea.europa.eu/highlights/copenhagen-beats-bristol-and-frankfurt. Accessed 22 April 2014.

Gredilla, A., Amigo, J. M., Fdez-Ortiz de Vallejuelo, S., de Diego, A., Bro, R., & Madariaga, J. M. (2012). Practical comparison of multivariate chemometric techniques for pattern recognition used in environmental monitoring. *Analytical Methods, 4*, 676–684.

Hallberg, R. O. (1991). Environmental implications of metal distribution in Baltic Sea sediments. *Ambio, 20*, 309–316.

Hansson, S. V., Rydberg, J., Kylander, M., Gallagher, K., & Bindler, R. (2013). Evaluating paleoproxies for peat decomposition and their relationship to peat geochemistry. *The Holocene, 23*, 1666–1671.

Haworth, E. Y., & Lund, J. W. G. (1984). *Lake sediments and environmental history—studies in paleolimnology and paleoecology in honour of Winifred tutin*. Minneapolis: University of Minnesota Press.

Kido, Y., Koshikawa, T., & Tada, R. (2006). Rapid and quantitative major element analysis method for wet fine-grained sediments using an XRF microscanner. *Marine Geology, 229*, 209–225.

Last, W. M., & Smol, J. P. (2004). *Tracking environmental change using lake sediments—volume 1: basin analysis, coring, and chronological techniques*. Dordrecht: Kluwer Academic Publishers.

Livingstone, D. A. (1955). A lightweight piston sampler for lake deposits. *Ecology, 36*, 137–139.

Löwenmark, L., Chen, H.-F., Yang, T.-N., Kylander, M., Yu, E.-F., Hsu, Y.-W., Lee, T.-Q., Song, S.-R., & Jarvis, S. (2011). Normalizing XRF-scanner data: a cautionary note on the interpretation of high-resolution records from organic-rich lakes. *Journal of Asian Earth Sciences, 40*, 1250–1256.

Lyons, W. B., & Harmon, R. S. (2012). Why urban geochemistry? *Elements, 8*, 417–422.

Matys Grygar, T., Sedláček, J., Bábek, O., Nováková, T., Strnad, L., & Mihaljevič, M. (2012). Regional contamination of Moravia (South-Eastern Czech Republic): temporal shift of Pb and Zn loading in fluvial sediments. *Water, Air, and Soil Pollution, 223*, 739–753.

Molin Christensen, J., & Holst, E. (1988). Evaluation of blood lead levels in Danes for the period 1976–1987. *Fresenius' Zeitschrift für Analytische Chemie, 332*, 710–713.

Nicholson, F. A., Smith, S. R., Alloway, B. J., Carlton-Smith, C., & Chambers, B. J. (2003). An inventory of heavy metals inputs to agricultural soils in England and Wales. *Science of the Total Environment, 311*, 205–219.

Nriagu, J. O. (1979). Global inventory of natural and anthropogenic emissions of trace metals to the atmosphere. *Nature, 279*, 409–411.

Nriagu, J. O., & Pacyna, J. M. (1988). Quantitative assessment of worldwide contamination of air, water and soils by trace metals. *Nature, 333*, 134–139.

Olsen, J., Björck, S., Leng, M. J., Gudmundsdóttir, E. R., Odgaard, B. V., Lutz, C. M., Kendrick, C. P., Andersen, T. J., & Seidenkrantz, M.-S. (2010). Lacustrine evidence of Holocene environmental change from three Faroese lakes: a multiproxy XRF and stable isotope study. *Quaternary Science Reviews, 29*, 2764–2780.

Passos, E. A., Alves, J. C., dos Santos, I. S., Alves, J. D. P. H., Garcia, C. A. B., & Spinola Costa, A. C. (2010). Assessment of trace metals contamination in estuarine sediments using a sequential extraction technique and principle components analysis. *Microchemical Journal, 96*, 50–57.

Quinn, G. P., & Keough, M. J. (2013). *Experimental design and data analysis for biologists*. New York: Cambridge University Press.

Reid, M. K., & Spencer, K. L. (2009). Use of principle components analysis (PCA) on estuarine sediment datasets: the effect of data pre-treatment. *Environmental Pollution, 157*, 2275–2281.

Renberg, I. (1986). Concentration and annual accumulation values of heavy metals in lake sediments: their significance in studies of the history of heavy metal pollution. *Hydrobiologia, 143*, 379–385.

Selig, U., & Leipe, T. (2008). Stratigraphy of nutrients and metals in sediment profiles of two dimictic lakes in North-Eastern Germany. *Environmental Geology, 55*, 1099–1107.

Skaarup, B., Westerbeek Dahl, B., & Thorning Christensen, P. (1998). *The fortifications of Copenhagen: a guide to 900 years of fortifications history*. Copenhagen: National Forest and Nature Agency, Danish Ministry of the Environment and Energy.

Smol, J. P. (2008). *Pollution of lakes and rivers—a paleoenvironmental perspective* (2nd ed.). Malden: Blackwell Publishing.

Templ, M., Filzmoser, P., & Reimann, C. (2008). Cluster analysis applied to regional geochemical data: problems and possibilities. *Applied Geochemistry, 23*, 2198–2213.

Tjallingii, R., Röhl, U., Kölling, M., & Bickert, T. (2007) Influence of water content on X-ray fluorescence core-scanning measurements in soft marine sediments. *Geochemistry, Geophysics, Geosystems, 8*. doi:10.1029/2006GC001393.

Vasskog, K., Paasche, Ø., Nesje, A., Boyle, J. F., & Birks, H. J. B. (2012). A new approach for reconstructing glacier variability based on lake sediments recording input from more than one glacier. *Quaternary Research, 77*, 192–204.

von Storch, H., Costa-Cabral, M., Hagner, C., Feser, F., Pacyna, J., Pacyna, E., & Kolb, S. (2003). Four decades of gasoline lead emission and control policies in Europe: a retrospective assessment. *Science of the Total Environment, 311*, 151–176.

Walraven, N., van Os, B. J. H., Klaver, G. Th., Middelburg, J. J., & Davies, G. R. (2014). Reconstruction of historical atmospheric Pb using Dutch urban lake sediments: a Pb isotope study. *Science of the Total Environment, 484*, 185–195.

Weltje, G. J., & Tjallingii, R. (2008). Calibration of XRF core scanners for quantitative geochemical logging of sediment cores: theroy and application. *Earth and Planetary Science Letters, 274*, 423–438.

Wold, S., Esbensen, K., & Geladi, P. (1987). Principle component analysis. *Chemometrics and Intelligent Laboratory Systems, 2*, 37–52.

Zitko, V. (1994). Principle components analysis in the evaluation of environmental data. *Marine Pollution Bulletin, 28*, 718–722.

Zupan, M., Einax, J. W., Kraft, J., Lobnik, F., & Hudnik, V. (2000). Chemometric characterization of soil and plant pollution: part 1: multivariate data analysis and geostatistical determination of relationship and spatial structure of inorganic contaminants in soil. *Environmental Science and Pollution Research, 7*, 89–96.